Design and Analysis of a Bearingless Permanent-Magnet Machine with Improved Torque Density for Stirred Tank Bioreactor

Ying Zhang, Yonghong Huang*, Ye Yuan, Jianhua Luo, and Xiaodong Chen

Abstract—A novel bearingless stirring permanent-magnet (PM) (BSPM) machine is proposed in this paper, which can offer high torque density, high efficiency, simple structure, and low cost. The novelty of the proposed machine is to provide a clean environment and no pinch-off areas in a stirred tank bioreactor and integrate appropriate magnetization directions of the PMs in the rotor. Firstly, the topology and operational principle of the proposed machine are described in detail. Then, the machine is designed for a given set of specifications, and its electromagnetic performances are analyzed by time-stepped transient finite-element method (FEM). Next, after the analysis of loss, a thermal simulation is established, complying with the design requirements. Finally, the efficiency and power factor map of the proposed BSPM machine are simulated for validation.

1. INTRODUCTION

Nowadays, with the development of the economy, it is difficult to support the requirements of mankind merely based on the supply of petrochemical resources [1]. Therefore, the utilization of biological resources has been focused and investigated by many scholars [2]. Furthermore, it should be noted that animal cell suspension culture, which has become an important part of industrial production, is the major source of biological resources. Bioreactor acting as the key equipment of cell suspension culture is an important part of maintaining cell growth [3]. Because animal cells are easily damaged in the process of cell suspension culture, bioreactor applications need high sealing and gnotobasis [4]. However, until now, a bearing machine is still commonly used in conventional bioreactors which has a lot of problems [5, 6]. First, it needs repair and maintenance from time to time, which will bring about liquid pollution in the bioreactor. Then, pinch-off areas will also be generated by using bearing topology, which will increase the possibility of cell destruction. However, by adopting a bearingless machine as a bioreactor stirrer, the aforesaid shortcomings are able to be conquered [7]. The bearingless machine is advantageous over a mechanical bearing machine in high requirements of clean environment and no pinch-off areas [8–11]. Since bearingless machines can magnetically levitate rotor, shaft and additional mechanical bearings are not required in their topologies. Hence, this machine is completely free of lubrication and does not suffer from abrasion, which guarantees long life time and low maintenance costs of the machine in bioreactor. The purpose of this paper is to apply a bearingless machine into the field of bioreactor stirrer and improve its torque density further. Therefore, a new PM array is proposed in this paper as shown in Fig. 1 together with that of an existing design.

In this paper, a novel 6-slot/16-pole exterior bearingless stirring permanent-magnet (PM) (BSPM) machine with Halbach PM array will be designed for a bioreactor with volume equaling to 400 L approximately. The topology and operational principle of the proposed BSPM machine will be described in Section 2. Then, in Section 3, by using Maxwell software, the dependable design and performance

optimization of a BSPM machine will be shown in detail. After that, the magnetic performance of the proposed BSPM machine will be illustrated in Section 4. Next, the simulated results will be given to verify the design requirements. Finally, the conclusions will be drawn based on the preamble analysis in Section 5.

2. MACHINE SPECIFICATION AND OPERATIONAL PRINCIPLE

2.1. Machine Specification

The cross section of a stirred tank bioreactor is shown in Fig. 2, in which a BSPM machine adopting an exterior rotor topology is installed. As shown in Fig. 3, the proposed BSPM machine is composed of 6 stator slots and 16 PMs. Furthermore, it is worth noting that the BSPM machine is installed at the bottom of a tank, which is beneficial to creating no unexpected flow-low regions. Besides, high torque density can be obtained by adopting exterior rotor construction and halbach magnetizing. It should be noted that the Halbach PM array adopted in the proposed machine is able to increase the torque density and reduce the harmonics of back-EMF. Concentrated-winding structure is also adopted in the proposed BSPM machine to increase torque density. In addition, this proposed machine offers a three-phase bearing force levitating the rotor. And a three-phase drive control also makes sure that the proposed BSPM machine rotates smoothly without large torque ripple.
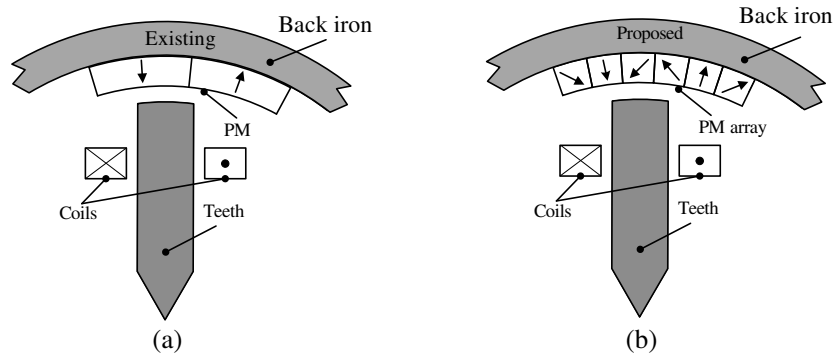

Figure 1. Schematics of existing and proposed PM arrays for high torque density BSPM machines. (a) Existing. (b) Proposed.
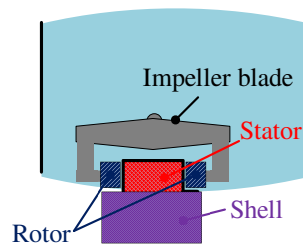

Figure 2. Cross section of a stirred tank bioreactor with a BSPM machine.

2.2. Bearing Forces and Torque

At present, a double-winding structure which has two sets of windings superimposed on the stator teeth is adopted by most bearingless machines. One provides electromagnetic torque, and the other provides levitation force. However, in the proposed BSPM machine, a set of windings making the rotor rotate and suspend at the same time is adopted. The structure of the single winding not only is simple, but also reduces the occurrence of machine failure to some extent.
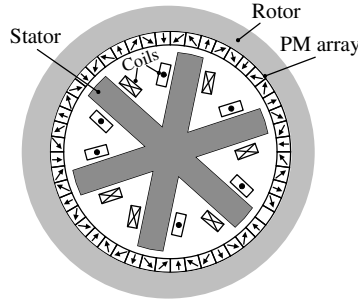
Figure 3. Proposed bearingless machine for a stirred tank bioreactor.

The passive control having 1-axis degrees of freedom and 2-rotated degrees of freedom can be obtained by adopting this winding topology. Moreover, the radial control which has 2 degrees of freedom can also be obtained. In the axial and rotated directions, the principle of passive suspension control can be illustrated in Fig. 4. Besides, it should be noted that the proposed topology has sufficient reluctance forces to stabilize the axial position and tilting. When the axial displacement occurs, the magnetic force will pull the rotor back to the equilibrium position. In the radial direction, the active suspension can stabilize the 2 degrees of freedom. It is worth noting that the model of levitation force has close relationship with the winding number and current. Each coil creates the radial and tangential forces, and their superposition leads to the total composite bearing force. The mathematical model of each coil n can be obtained as follows:

$$\begin{cases} F_{n,x}(\theta_r) = k_x \cdot [\cos(n-1) \cdot 60° + \sin(n-1) \cdot 120°] \cdot \cos[(n-1) \cdot 120° + \theta_r] \cdot N \cdot I_{ni} \\ F_{n,y}(\theta_r) = k_y \cdot [\sin(n-1) \cdot 60° + \cos(n-1) \cdot 120°] \cdot \sin[(n-1) \cdot 120° + \theta_r] \cdot N \cdot I_{ni} \end{cases} \quad (1)$$

where k_x and k_y represent the force factor in the x-direction and y-direction, respectively, and N is the number of windings, I_{ni} the current suspension component and θ_r the electrical rotor angle.
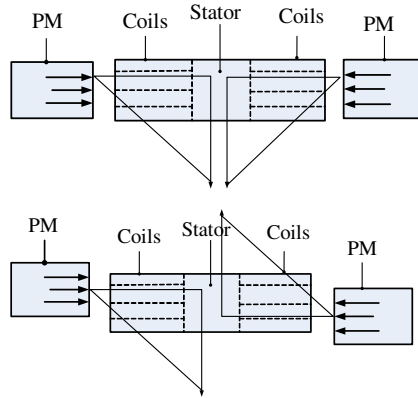

Figure 4. The control of the passive suspension.

As a result, the total composite bearing force in x-direction and y-direction can be derived as follows:

$$\begin{cases} F_x = \sum_{n=1}^{6} F_{n,x} \cos[\theta_r + 60°(n-1)] \\ F_y = \sum_{n=1}^{6} F_{n,y} \sin[\theta_r + 60°(n-1)] \end{cases} \quad (2)$$

For BSPM machines, only specific stator magnetomotive harmonic, known as working harmonic, interacts with the PM field to produce continuous electromagnetic torque [12]. The torque generated

by each coil n in the proposed BSPM machine can be given by

$$T_n(\alpha) = n_T \cdot \sin^2(p \cdot \alpha + (n-1) \cdot 120°) \cdot N \cdot I_{mi} \tag{3}$$

where α is the mechanical angle, p the magnet pole-pair number, n_T the factor of drive current, and I_{mi} the current torque component. As a result, the total torque of BSPM machines can be derived as follows:

$$T = \sum_{n=1}^{6} T_n = 3 \cdot n \cdot T \cdot N \cdot I_{mi} \tag{4}$$

3. MACHINE DESIGN

The relationship between maximum electromagnetic torque and electromagnetic load can be obtained as follows:

$$T_{em\ \max} = \frac{\sqrt{2}\pi}{4} B_{\delta 1} L_{ef} D_{i1}^2 A \times 10^{-4} \tag{5}$$

where $B_{\delta 1}$ is the amplitude of air-gap flux density, L_{ef} the axial length of BSPM machine, D_{i1} the diameter of stator, and A the effective value of electrical load. When the electromagnetic load is selected, the main dimensions of BSPM machines can be derived as:

$$D_{i1}^2 L_{ef} = \frac{4T_{em\ \max} \times 10^{-4}}{\sqrt{2}\pi B_{\delta 1} A} \tag{6}$$

The leading design parameters of the basic module of the proposed machine are defined in Fig. 5. The choice of these parameters can be guided by the sizing equation and should follow a number of design criterions [13, 14]. The ratio between axial length and diameter in BSPM machine can be expressed as:

$$\lambda = \frac{L_{ef}}{D_i}, \tag{7}$$

it is within the range from 0.6 to 0.7 in BSPM machines. Considering the rated torque, rated speed and restrictions of the container size, the stator outside diameter and axial length are about 116 mm and 74 mm, respectively.

For the proposed machine, these parameters in Fig. 5 play a key role in its electromagnetic performance. So, it is very important to optimize these parameters, determined by considering their effect on back-EMF and other performance indicators, such as torque and inductances. The air-gap length in BSPM machines is defined as δ_g. The thickness of the rotor encapsulation δ_1 is 1 mm, the thickness of the stator encapsulation δ_2 1 mm, and the thickness of tank wall δ_3 1 mm. To keep the fluid
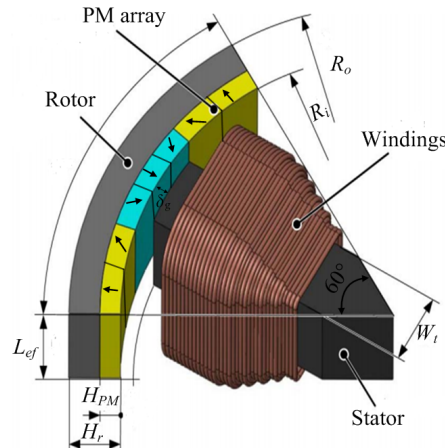

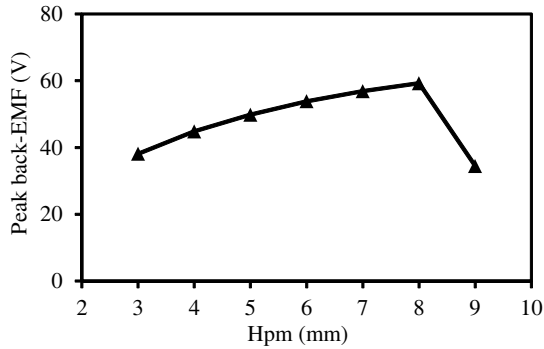**Figure 5.** Definition of leading machine design parameters.

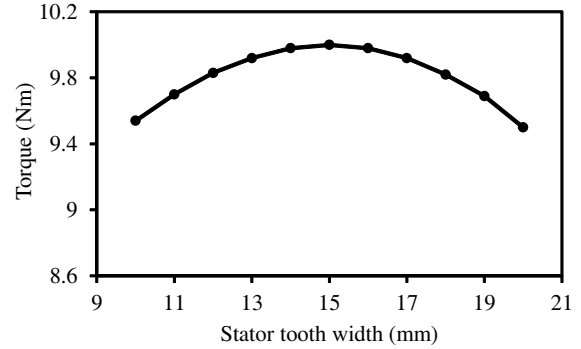**Figure 6.** Variation of peak back-EMF with H_{pm}.

Figure 7. Variation of torque with stator tooth width.

sheer forces low, a fluid gap δ_4 equal to 2 mm should also be required. Therefore, the air-gap of BSPM machine can be obtained as follows:

$$\delta_g = \delta_1 + \delta_2 + \delta_3 + \delta_4 = 5\,\text{mm} \tag{8}$$

In addition, the effect of the thickness of PM H_{pm} on the back-EMF is illustrated in Fig. 6. It should be noted that the peak back-EMF is increased by raising H_{pm}. However, if H_{pm} is too large, the remaining back iron gets saturated. Therefore, the stronger PMs do not result in higher magnetic flux density. And the maximum back-EMF can be obtained when H_{pm} equals 8 mm. The last main design parameter is the stator tooth width W_t. As shown in Fig. 7, the coherence between W_s and torque is depicted. It should be noted that the general trend of torque is increasing-deceasing. And the maximum torque is able to be obtained when W_s is equal to 15 mm. Based on Maxwell software, the optimal parameters is listed in Table 1.

4. PERFORMANCE EVALUATION

4.1. Winding Topology and Field Distributions

The slot electrical potential star vectogram is shown in Fig. 8(a). It is seen that Phases A, B, and C mutually differ 120 degrees. Based on Fig. 8(a), stator winding connection in BSPM machines can be obtained (see Fig. 8(b)). As shown in Fig. 9, the air-gap flux density of proposed machine is analyzed by FEM and compared with that of the existing one. It can be seen from Fig. 9 that the proposed machine has higher magnetic flux density than the existing one. Furthermore, as shown in Fig. 9(b), the 8th harmonic is the working harmonic generating torque, and 4th, 14th, 16th, 20th, and 26th are tooth harmonics, which are the main source of generating magnet eddy current (EC) loss.
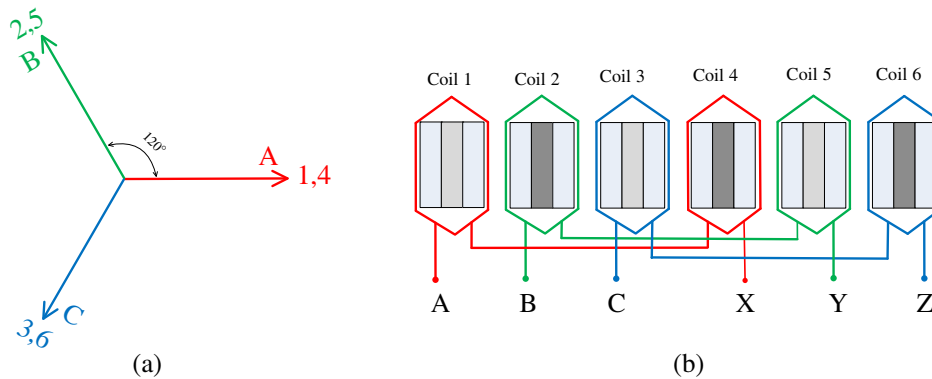

Figure 8. Stator winding arrangement. (a) Slot electrical potential star vectogram. (b) Winding connection.

Table 1. Design parameters of existing machines.

Parameter	Symbol	Value
Rated power	P	500 W
Slot number	q	6
Pole-pair number	p	8
Outer rotor radius	R_o	76 mm
Inner rotor diameter	R_i	63 mm
Axial length	L	74 mm
Magnet thickness	H_{PM}	5 mm
Stator tooth width	W_t	15 mm
Air-gap thickness	δg	5 mm
Rotor thickness	H_r	13 mm
Rated speed	n	500 r/min
Rated torque	T	10 Nm
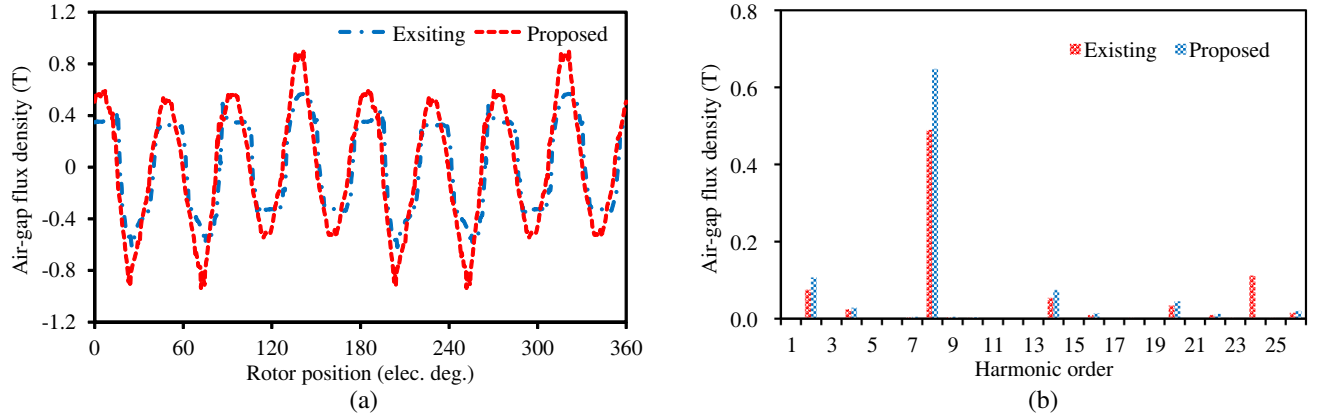
Figure 9. Comparison of air-gap flux density and harmonic spectra. (a) Air-gap flux density. (b) Harmonic spectra.
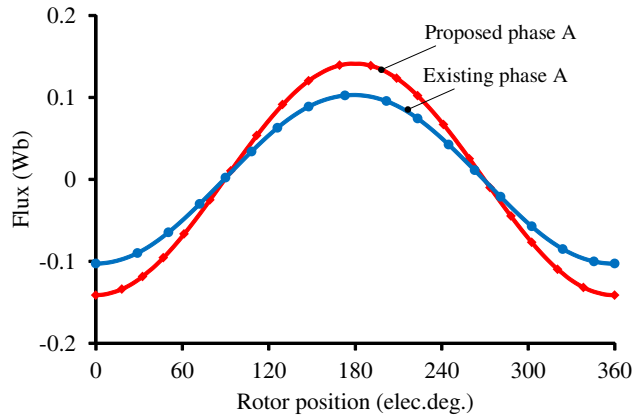
Figure 10. Comparison of PM flux linkages.
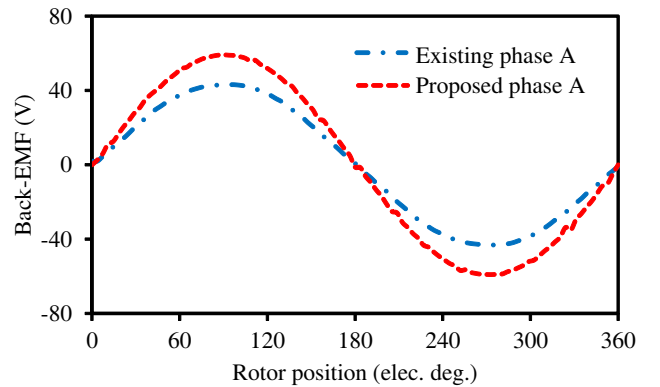
Figure 11. Comparison of phase back-EMF.

4.2. Flux Linkage, Back-EMF and Inductance

The FEM-predicted PM flux linkages are illustrated in Fig. 10. It is seen that the flux linkage of the proposed machine is greater than that of the existing machine.

The phase back-EMF E can be expressed as

$$E = \frac{d\psi}{dt} = \frac{d\psi}{dx}v \tag{9}$$

Therefore, it can be obtained from Eq. (9) that the back-EMF is only connected with the rate of change in the flux linkage. Since the amplitude of flux linkage in the proposed machine is greater than that in existing machine, the back-EMF of the proposed machine is also greater than that of existing machine as shown in Fig. 11.

The self- and mutual-inductances of each phase can be predicted by FEM as well, as shown in Fig. 12. For example, the self- and mutual-inductances of phase-A are calculated as

$$\begin{cases} L_{aa} = \dfrac{\psi_A(I_b = I_c = 0, I_a = I) - \psi_A(I_a = I_b = I_c = 0)}{I} \\ M_{ab} = \dfrac{\psi_B(I_b = I_c = 0, I_a = I) - \psi_A(I_a = I_b = I_c = 0)}{I} \\ M_{ac} = \dfrac{\psi_C(I_b = I_c = 0, I_a = I) - \psi_A(I_a = I_b = I_c = 0)}{I} \end{cases} \tag{10}$$
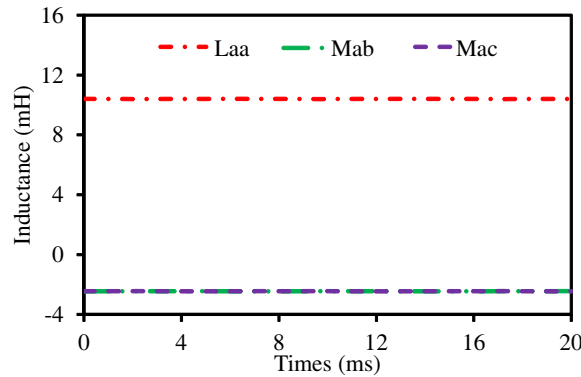

Figure 12. Comparison of self- and mutual-inductances.

4.3. Torque, Loss and Thermal Analysis

Because Halbach structure is beneficial to improving the ability of magnetic congregate effect, the torque of the proposed machine is obviously greater than that of the existing machine, as shown in Fig. 13. Furthermore, it can also be seen from Fig. 13 that the torque has linear growth when the range of Q-axis current is from 0 to 36 A, which indicates that the proposed BSPM machine has overload ability.
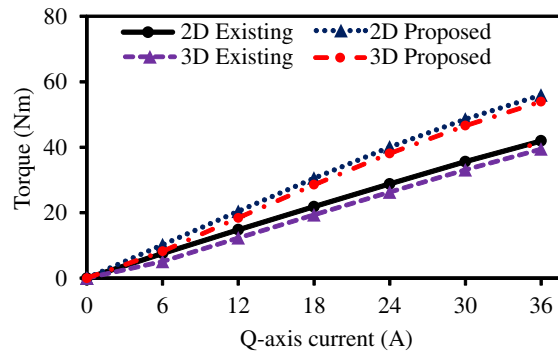

Figure 13. Comparison of torque variations with Q-axis current.

Finally, it should be noted that the results calculated by 2D FEM are in a good agreement with 3D FEM.

High temperature of the machine not only damages the lifetime of the machine, but also affects the environment of a stirred tank bioreactor. Hence, in order to analyze the thermal properties of the proposed BSPM machine, the occurring loss needs to be determined. Iron losses including hysteresis loss, EC loss and excess loss are generated in the stator and rotor owing to the change of magnetic fields [15]. In addition, due to cogging effect and ample magnetomotive force (MMF) harmonics in BSPM machines, magnet EC loss does exist in BSPM machines [16–18]. Besides, copper loss will also be generated in the stator windings [19]. Taking the circumferential and radial components of magnetic flux density variation into consideration, the iron loss in watts per kilogram can also be derived as in Fig. 4.

$$
P_{Fe} = \sum_{i=1}^{n} K_c \cdot (i^2 \cdot f^2) \cdot (B_{r,\,i}^2 + B_{t,\,i}^2) + K_h \cdot f \cdot
\left[
\begin{array}{l}
B_{t,\,m}^2 \cdot \left(1 + c \cdot \frac{1}{B_{t,\,m}} \sum_{i=1}^{N} \Delta B_{t,i}\right) \\[2mm]
+ B_{r,\,m}^2 \cdot \left(1 + c \cdot \frac{1}{B_{r,\,m}} \sum_{i=1}^{N} \Delta B_{r,i}\right)
\end{array}
\right]
$$
$$
+ K_e \cdot (i^{1.5} \cdot f^{1.5}) \cdot (B_{r,\,i}^{1.5} + B_{t,\,i}^{1.5})
\tag{11}
$$

where K_h, K_c, and K_e are the coefficients of hysteresis loss, EC loss, and excess loss, respectively; f is the fundamental frequency; $B_{t,i}$ and $B_{r,i}$ are amplitude of the ith harmonic of the tangential and radial magnetic flux density, respectively; $B_{t,m}$ and $B_{r,m}$ are the maximum value of the ith harmonic of the tangential and radial magnetic flux density, respectively. Finally, the total iron loss can be given by the sum of every part of BSPM machines. Fig. 14 compares the variations of stator and rotor iron loss with respect to rotor speed for which the same method and lamination steel characteristic as given in Table 2

Table 2. Material characteristics (M19-29G).

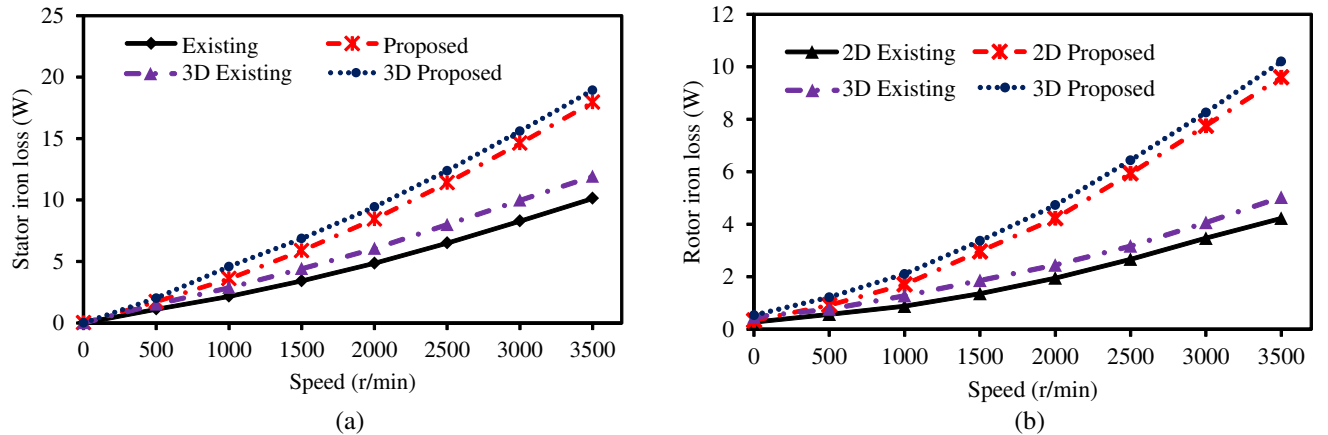| Name	Value
Lamination density δ (kg/m^3)	7872
Lamination thickness d (mm)	0.35
Stacking factor	0.94
Stacking direction	z-axis
Loss constant k_h	184.23
Loss constant k_c	0.39
Loss constant k_e	0.27

Figure 14. Variation of iron loss with respect to rotor speed. (a) Stator iron loss. (b) Rotor iron loss.
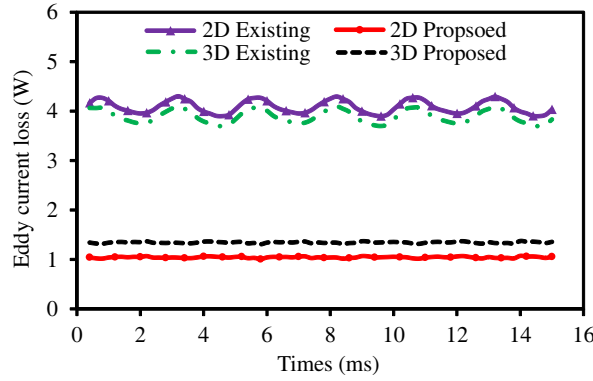
Figure 15. Comparison of eddy current loss at rated speed 500 r/min.

are employed. It is seen that the general trend of stator and rotor iron loss with respect to speed is in parabolic growth. Since the air-gap flux density generated by the proposed machine is greater than that of the existing machine, the iron loss of the proposed machine both in stator and rotor is slightly greater than that of the existing machine. Furthermore, the magnet EC loss caused by asynchronous harmonics can also be calculated as follows:

$$P_{PM} = \sum_{h=1}^{\infty} \left(\int_{PM} \frac{|J_h|^2}{2\sigma} dv \right) \tag{12}$$

where J_h and σ are the EC density of hth harmonics and conductivity, respectively. Fig. 15 makes a comparison of magnet EC loss between the proposed machine and existing machine at rated speed 500 r/min. It is worth noting that the magnet EC loss of existing machine is lower than that of the proposed machine, which is due to the segmentation of PMs. Magnet segmentation is conducive to cutting the EC path, thus decreasing magnet EC density. In addition, it is well known that copper loss is the main source for machine loss. Based on Joule's law, it depends on the resistance and the current flowing through it [20]. The copper loss can be calculated as follows:

$$P_{Cu} = 6 \cdot R \cdot (2n^2 - 2n + 1) \cdot (I_{d,rms} + I_{b,rms})^2 \tag{13}$$

where R is the coil resistance; $I_{d,rms}$ and $I_{b,rms}$ are the rms value of the drive current and bearing current, respectively; n represents the ratio between the drive and bearing currents.

Ultimately, the efficiency η of the proposed machine is given by

$$\eta = \left(1 - \frac{\sum p}{p_2 + \sum p} \right) \times 100\% \tag{14}$$

$$\sum p = p_{Fe} + p_{Cu} + p_{Pm} + p_\Omega + p_{ad} \tag{15}$$

where P_2 is the output power, ΣP the total loss, P_{Fe} the total iron loss, P_{Cu} the copper loss, P_{Pm} the magnet EC loss, P_Ω the mechanical loss, and P_{ad} the stray loss. The efficiency map and power factor map of the proposed BSPM machine are shown in Fig. 16. When the speed is from 0 to 500 r/min, the machine operates at constant torque. When the speed is from 500 to 2000 r/min, the machine operates at constant power. Finally, at rated condition, it can be seen from Fig. 16(a) and Fig. 16(c) that the efficiency and power factor of the proposed BSPM machines are 0.97 and 0.77, respectively. In this paper, efficiency map is calculated by Ansoft script. In fact, it is calculated by many points, and these points also paint a cloud picture after processing. Actually, there are no data on both sides of the small area. Therefore, there does exist some problems at almost zero speed and low torque region. However, it has little effect on our calculation, because the machine cannot operate at this region for a long time. Furthermore, Fig. 16(b) illustrates the total loss in contour plot over torque-speed range. It can be obviously seen that the total loss is increased with the increase of rotor speed.

In addition, suited temperature is also very important for BSPM machines in stirred tank bioreactor. Hence, the thermal analysis of the proposed BSPM machine is carried out by using Motor-CAD software, whose calculation is based on thermal circuit. Firstly, the geometrical parameters of the
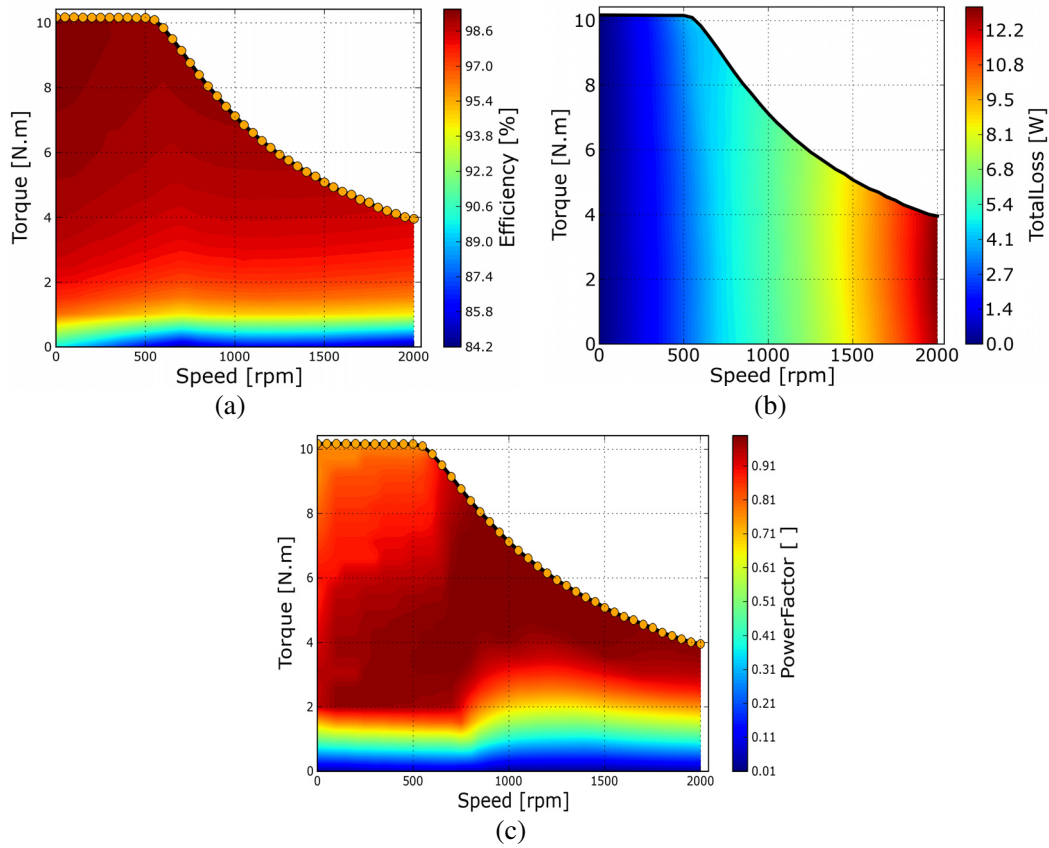
Figure 16. Efficiency, total loss map and power factor map. (a) Efficiency. (b) Total loss. (c) Power factor.
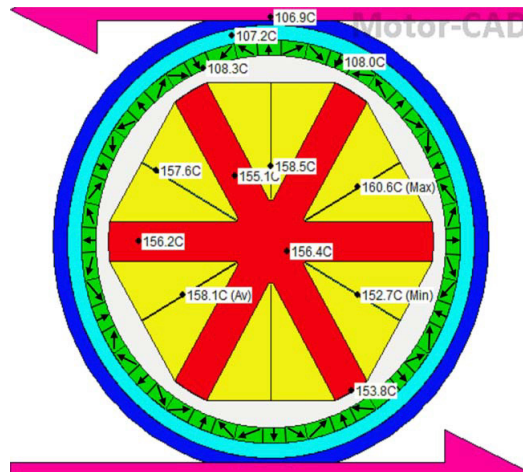

Figure 17. Thermal analysis of the proposed machine.

BSPM machine and windings should be input into the geometry sections of Motor-CAD. The cross-section views of the SWBFM in Motor-CAD can be illustrated below in Fig. 17. Moreover, it should also be noted that the material for the housing is chosen as the default aluminum alloy 195 cast, and the copper winding is specified as pure copper. M19-29G material is adopted for the stator and rotor core. In addition, it is also worthy of noticing that the interface values and contact resistance between different materials, the radiation effect, and the natural convection around the motor exterior are specified as

default Motor-CAD values. Next, it can be seen from Fig. 17 that the rotor temperature of the proposed machine operating at rated condition is 106.9°C, which indicates that it complies with the environment of bioreactor tank. Also, the average temperature of stator and windings are approximately equal to 155°C and 158°C. Finally, it can be seen that the maximum temperature of PMs is 108°C, which cannot increase the risk of PMs irreversible demagnetization. Compared with practical temperature, the indoor temperature and wind is the source to affect the accuracy of simulated results. However, it is able to be neglected within error. In general, according to thermal analysis, it can be concluded that the proposed BFPM machine can operate well without overlarge heat.

5. CONCLUSIONS

In this paper, a novel BSPM machine that employs a clean environment, no pinchoff areas in a stirred tank bioreactor and appropriate magnetization directions of the PMs in the rotor has been described. Based on simulated results, it is shown that the proposed machine exhibits high torque density with relatively large air-gap necessary for the targeted application in a stirred tank bioreactor. A thermal analysis reveals that the loss is in an acceptable range for rated operation condition so that there is no negative effect on the bioreactor application. Hence, the proposed BSPM machine is especially competent for bioreactor stirring applications.

ACKNOWLEDGMENT

REFERENCES

1. Montiel-Moreno G., J. Zechinelli-Martini, and G. Vargas-Solar, "SLSELS: Semantic integration system for exploitation of biological resources," *2009 Mexican International Conference on Computer Science*, 197–202, 2010.

2. Artis, F., D. Dubuc, J. Fournie, M. Poupot, and K. Grenier, "Microwave dielectric spectroscopy for biological cells suspensions analysis and proliferation evaluation," *2014 44th European Microwave Conference*, 275–278, 2014.

3. Daniele, M., F. Vozzi, A. Cisternino, G. Vozzi, and A. Ahluwalia, "A high-throughput bioreactor system simulating physiological environments," *IEEE Transactions on Industrial Electronics*, Vol. 55, No. 10, 3273–3280, 2008.

4. Maki, A., T. Ryynanen, J. Verho, J. Kreytzer, J. Lekkala, and P. J. Kallio, "Indirect temperature measurement and control method for cell culture devices," *IEEE Transaction on Automation Science and Engineering*, Vol. 1, No. 99, 1–10, 2016.

5. Henson, M. A., "Biochemical reactor modeling and control," *IEEE Control Systems Magazine*, Vol. 26, No. 4, 54–62, 2006.

6. Ye, S., and K. T. Chau, "Chaoization of DC motors for industrial mixing," *IEEE Transactions on Industrial Electronics*, Vol. 54, No. 4, 2024–2032, 2007.

7. Bartholet, M. T., T. Nussbaumer, S. Silber, and J. W. Kolar, "Comparative evaluation of polyphase bearingless slice motors for fluid-handling applications," *IEEE Transactions on Industry Applications*, Vol. 45, No. 5, 1821–1830, 2009.

8. Park, S. and C. Lee, "Decoupled control of a disk-type rotor equipped with a three-pole hybrid magnetic bearing," *IEEE/ASME Transactions on Mechatronics*, Vol. 15, No. 5, 793–804, 2010.

9. Ooshima, M., A. Chiba, T. Fukao, and M. A. Rahman, "Design and analysis of permanent magnet-type bearingless motors," *IEEE Transactions on Industrial Electronics*, Vol. 43, No. 2, 292–299, 1996.

10. Yang, S. and M. Huang, "Design and implementation of a magnetically levitated single-axis controlled blood pump," *IEEE Transactions on Industrial Electronics*, Vol. 56, No. 6, 2213–2219, 2009.

11. Reichert, T., T. Nussbaumer, W. Gruber, and J. W. Kolar, "Bearingless Permanent-Magnet motor with 4/12 slot-pole ratio for bioreactor stirring applications," *IEEE/ASME Transactions on Mechatronics*, Vol. 16, No. 3, 431–439, 2011.

12. Dajaku, G., W. Xie, and D. Gerling, "Reduction of low space harmonics for the fractional slot concentrated windings using a novel stator design," *IEEE Transaction on Magnetics*, Vol. 50, No. 5, 1–12, 2014.

13. Jian, L. and K. T. Chau, "Design and analysis of a magnetic geared electronic-continuously variable transmission system using finite element method," *Progress In Electromagnetics Research*, Vol. 107, 47–61, 2010.

14. Jian, L., G. Xu, Y. Gong, J. Song, J. Liang, and M. Chang, "Electromagnetic design and analysis of a novel magnetic-gear-integrated wind power generator using time-stepping finite element method," *Progress In Electromagnetics Research*, Vol. 113, 351–367, 2011.

15. Bramerdorfer, G. and D. Andessner, "Accurate and easy-to-obtain iron loss model for electric machine design," *IEEE Transactions on Industrial Electronics*, Vol. 64, No. 3, 2530–2537, 2017.

16. Bianchi, N. and E. Fornasiero, "Impact of MMF space harmonic on rotor loss in fractional-slot permanent-magnet machines," *IEEE Transaction on Energy Conversion*, Vol. 24, No. 2, 323–328, 2009.

17. Chai, F., P. Liang, Y. Pei, and S. Cheng, "Magnet shape optimization of surface-mounted permanent-magnet motors to reduce harmonic iron losses," *IEEE Transaction on Magnetics*, Vol. 52, No. 7, Article ID: 7300504, 2015.

18. Choi, G. and T. M. Jahns, "Reduction of eddy-current losses in fractional-slot concentrated-windings synchronous PM machines," *IEEE Transaction on Magnetics*, Vol. 52, No. 7, Article ID: 8105904, 2016.

19. Gonzalez, D. A. and D. M. Saban, "Study of the copper losses in a high-speed permanent-magnet machine with form-wound windings," *IEEE Transactions on Industrial Electronics*, Vol. 61, No. 6, 3038–3045, 2014.

20. Kim, Y. and K. Nam, "Copper-loss-minimizing field current control scheme for wound synchronous machines," *IEEE Transactions on Power Electronics*, Vol. 32, No. 2, 1335–1345, 2017.